nature climate change

SUPPLEMENTARY INFORMATION

DOI: 10.1038/NCLIMATE1390

Limited forcing of glacier loss through land-cover change on Kilimanjaro

1 Supplementary Figures and Legends

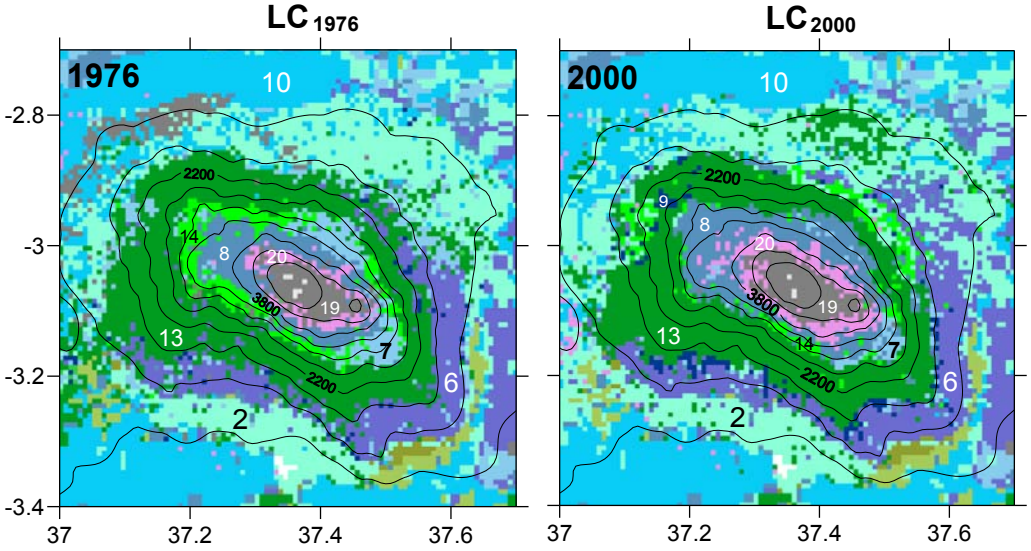

Figure S1: Land cover index of the USGS 24-class system on Kilimanjaro in the WRF atmospheric model domain 4 (longitude/latitude, contours in m) in 1976 and 2000. The main classes are 2 (dryland cropland), 6 (cropland/woodland mosaic), 7 (grassland), 8 (shrubland), 9 (mixed shrubland/grassland), 10 (savanna), 13 (evergreen broadleaf), 14 (evergreen needleleaf), 19 (barren), and 20 (herbaceous tundra). The bright grid cells in the summit area represent glacier cover, white cells in the southern lowland are Moshi Town. See Supplementary Methods (page S-3) for more details.

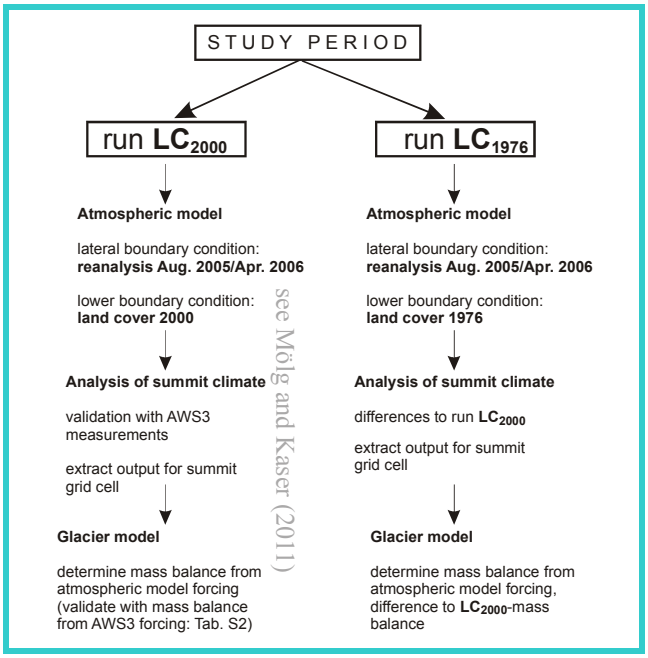

Figure S2: Summary sketch of the methodology used for each study period and each model setting (EX-REF, EX-SOI, EX-LMO). Run LC_{2000} precedes run LC_{1976}. Configuration and validation of LC_{2000} are covered by a separate paper (Mölg and Kaser, 2011) and are briefly summarized in the Supplementary Methods. Validation of the final quantity of interest (mass balance from atmospheric model forcing) is repeated in Tab. S2.

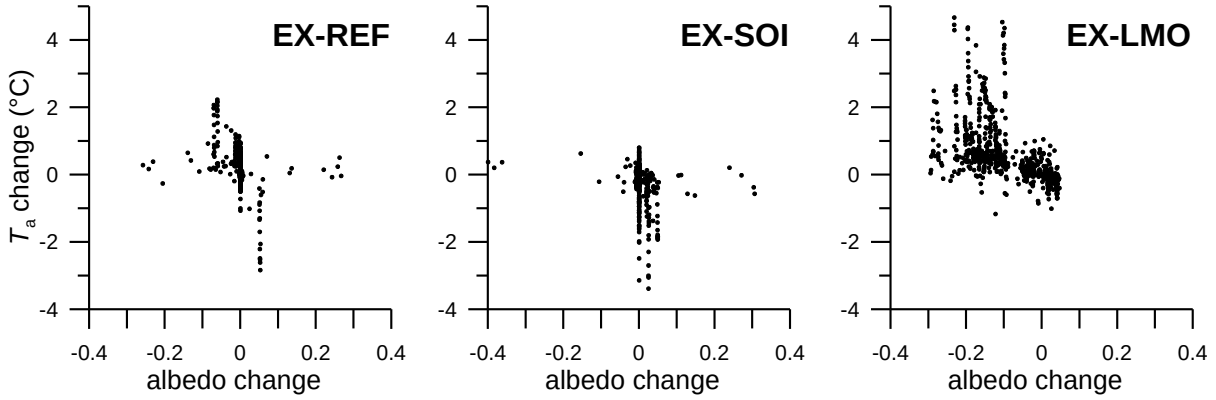

Figure S3: Scatterplots of hourly surface albedo change vs. 2-metre air temperature change (LC_{2000} minus LC_{1976}) in the wet season for the atmospheric models's glacierized summit grid cell. Experiments EX-REF and EX-SOI use the RUC land surface scheme, EX-LMO employs the Noah land surface scheme.

2 Supplementary Methods

Validation of the combined modelling system

As indicated in the main text, the models employed as well as their linkage were evaluated and confirmed in our previous studies.

Mölg et al. (2009) forced the mass balance model with 3-year records from AWS3 (5873 m, near the glacier top) between February 2005 and January 2008, and found a good agreement between measured and modelled (a) glacier surface temperature at AWS3, (b) surface height change and mass balance at AWS3, and (c) surface height change and snow depth at measurement sites further down-glacier (5760 and 5690 m). This means the "observed" mass balance estimate of Kersten Glacier is mostly, but not solely, constrained by AWS3 measurements.

Mölg and Kaser (2011) showed for the time slices of the present paper (August 2005, April 2006) that the WRF atmospheric model resolves the glacierized zone on Kilimanjaro in their set-up and reproduces AWS3 measurements well, i.e. conditions in the glacier's boundary layer: air temperature and humidity as well as wind speed at screen level, air pressure, precipitation sum and frequency, and cloud cover (see Fig. 6 in Mölg and Kaser, 2011). This was assessed by the explained variance in observations and the skill added by the model's high resolution. Using the atmospheric model output of the glacier's boundary layer as direct input to the mass balance model finally reproduced the observed mass balance estimate of Kersten Glacier. This means that uncorrected atmospheric model output (no statistical intervention) is a suitable forcing for a process-resolving MB model, an important advancement in the study of mountain cryosphere-climate relations (Mölg and Kaser, 2011). This final success is shown in Tab. S2 for the simulations presented here.

Interpolation of high-resolution vegetation data to WRF model domain 4

The detailed land use surveys of Hemp (2005, 2006) for the years 1976 and 2000 (georeferenced TIF files at 30 m spatial resolution) were first translated to the USGS 24-class system used by the WRF model as follows: montane forest – class 13; subalpine *Erica* cloud forest – class 14; *Erica* bush – class 8; *Helychrysum* cushion vegetation – class 20; grassland – class 7; clearings, forest regeneration – class 9; savanna – class 10; fields overgrown with bush – class 8; forest plantation – class 14; agriculture, shamba systems – class 2; homegardens – class 6 (see Fig. S1 caption for class names); These data are then interpolated to model domain 4 by nearest neighbor interpolation (Fig. S1). For areas not covered by Hemp's data (the margin of domain 4; not shown in Fig. S1) we maintain WRF's standard land cover data. Vegetation fraction is assigned to each class from the USGS data set as well (e.g., Table III in Sertel et al., 2010).

As detailed in Hemp (2005), the dominant changes since 1976 were the strong reduction of subalpine *Erica* forests (light green zone 14 on the mountain slope in the 1976 image, Fig. S1), which were mostly replaced by shrubland (zone 8 on slopes). Reduction of montane forests (dark green zone 13 in Fig. S1) was less severe and occurred in favour of dryland cropland (class 2) and cropland/woodland mosaic (class 6) extensions.

Glacier cover in WRF model domain 4

A glacier cell corresponds to USGS class 24, "snow and ice". This worked reasonably well for the RUC land surface scheme (EX-REF, EX-SOI), but in conjunction with the Noah land surface scheme the amplitude of the simulated diurnal cycle of 2-metre air temperature above the glacier was systematically too large compared to AWS3 observations (nocturnal cold bias). This problem was resolved by defining a glacier cell as "non-vegetated" surface (USGS class 19) with soil type 16 ("land ice"). This also yielded the closest similarity of grid cell-simulated energy fluxes to the energy fluxes revealed with the help of AWS3 measurements (Mölg et al., 2009). Thus, for WRF future studies that deal with small mountain glaciers surrounded by barren land, the Noah land surface together with land class 19 and soil class 16 can be recommended to simulate the glacier SBL, based on our results.

The three experiments and their differences in the atmospheric model

The same pair of runs (land cover distribution LC_{2000} vs. LC_{1976}) was repeated for three different model settings and each season, in order to test the robustness of results (e.g., Pitman et al., 2004). In addition to experiment EX-REF, we identify two crucial elements for the question of LCC.

First, it is well known that the initial soil moisture field impacts atmospheric model results, in particular the simulation of atmospheric flows over mountains (e.g., Rotach and Zardi, 2007). The EX-REF runs therefore start with the soil moisture field obtained after one month of integration by Mölg and Kaser (2011), to incorporate spatial variability in soil moisture. However, EX-REF uses identical initial soil moisture fields for LC_{2000} and LC_{1976} runs. Thus experiment EX-SOI uses the soil moisture

field from the end of EX-REF_LC_{2000} (EX-REF_LC_{1976}) as initial field for EX-SOI_LC_{2000} (EX-SOI_LC_{1976}). This means EX-SOI differs in land cover and initial soil moisture between LC_{2000} and LC_{1976} (i.e., mean initial soil moisture is higher for LC_{1976}).

Second, the land surface model employed in the atmospheric model; Experiment EX-LMO therefore starts with differing initial soil moisture (as EX-SOI) and, additionally, uses another land surface scheme. The RUC scheme for EX-REF and EX-SOI is described in detail in Smirnova et al., (1997) and solves heat and moisture transfer in the soil on six layers in the vertical (0, 5, 20, 40, 60, 300 cm depth). For EX-LMO the Noah land surface scheme with four layers in the vertical is employed (10, 30, 60, 100 cm depth) (Chen and Dudhia, 2001). Both schemes consider vegetation processes, soil water in different phases, and snow cover effects, which makes them suitable for the present study.

3 Supplementary Tables

Supplementary Table 1: The main user-specific settings in the WRF atmospheric model (see Skamarock et al. (2008) for details and references of the schemes). Differences between the three experiments (EX-REF, EX-SOI, EX-LMO) are indicated. Settings are from Mölg and Kaser (2011) except for the initial soil moisture, and for the land surface model in EX-LMO (see Section 2 above).

Feature or Component	**Setting**
horizontal grid spacing	39, 13, 3.25, 0.812 km (grids 1-4)
layers in the vertical	terrain-following (35)
lateral boundary condition	variable (ERA-Interim* at 0.7°, six-hourly)
top boundary condition	Rayleigh damping
grid nudging	yes (grid 1, 6-hourly), no (grids 2-4)
long time step	180, 60, 15, and 3.75 s (grids 1-4)
initial soil moisture	same for (adjusted to) recent and past land cover in **EX-REF** (in **EX-SOI** and **EX-LMO**)
land surface	RUC scheme (**EX-REF**, **EX-SOI**), Noah scheme (**EX-LMO**)
atmospheric surface layer	Monin-Obukhov scheme
planetary boundary layer	YSU scheme (wet season), MYJ scheme (dry season)
horizontal advection	explicit 6-th order
cloud microphysics	Thompson 7-class scheme
cumulus parameterization	Betts-Miller-Janjic (grids 1-3), none (grid 4)
radiation	Dudhia (shortwave) and CAM (longwave) schemes

* also used to define initial conditions (including three days of spin-up)

Supplementary Table 2: Glacier-wide specific mass balance on Kersten Glacier (kg m^{-2} $month^{-1}$) in August 2005 (dry season) and April 2006 (wet season) for the present glacier extent: Determinations with the distributed mass balance model from (a) AWS3 measurements as forcing and (b) forcing with output of the atmospheric model (domain 4 summit) in the three different experiments (recent land cover LC_{2000} as lower boundary).

	Forcing data			
	AWS3*	**EX-REF****	**EX-SOI**	**EX-LMO**
wet season	+39.1 ± 7.8	+37.6	+37.6	+36.9
dry season	–35.3 ± 7.0	–33.1	–38.0	–40.4

* Mölg et al. (2009) – summarized in Fig. 5 in Mölg and Kaser (2011)

** the runs presented in Mölg and Kaser (2011) (slightly changed initialization, see Section 2 above)

Supplementary Table 3: Simulated mean vertical gradients (per 100 m altitude) in air temperature, precipitation and wind speed between the two glacier grid cells that represent Kersten Glacier in domain 4 (5213 and 5573 m) in the different seasons and experiments. These three gradients are required as mass balance model parameters (Mölg et al., 2009).

	EX-REF		**EX-SOI**		**EX-LMO**	
	LC_{2000}	LC_{1976}	LC_{2000}	LC_{1976}	LC_{2000}	LC_{1976}
wet season						
air temperature (°C)	–0.65	–0.67	–0.70	–0.67	–0.84	–0.86
wind speed (m s^{-1})	0.13	0.12	0.12	0.12	0.01	0.00
precipitation (mm $month^{-1}$)	–3.9	–3.6	–4.8	–4.0	–2.8	–5.8
dry season						
air temperature (°C)	–0.69	–0.69	–0.69	–0.69	–0.76	–0.76
wind speed (m s^{-1})	0.25	0.24	0.25	0.25	0.26	0.25
precipitation (mm $month^{-1}$)	1.4	1.8	1.1	1.9	1.1	0.8

Supplementary Table 4: Simulated precipitation change (mm month^{-1}) due to LCC (LC_{2000} minus LC_{1976} runs) in the three different experiments for the summit grid cell (representing Kersten Glacier with AWS3), the summit zone (mean and sigma for all grid cells > 5400 m altitude), and the Northern Icefield grid cell in the wet and dry season. Wet-season (dry-season) mean and sigma for changes on the two glacier grid cells yield –4 ± 8 (–4 ± 3) mm month^{-1}.

Experiment	Kersten Glacier	summit zone	Northern Icefield
EX-REF	–5.7 (wet)	–2.6 ± 3.8 (wet)	+0.5 (wet)
	–1.5 (dry)	+1.6 ± 4.9 (dry)	+0.3(dry)
EX-SOI	–13.5 (wet)	–13.6 ± 5.4 (wet)	–8.7 (wet)
	–7.3 (dry)	–6.3 ± 1.5 (dry)	–6.7 (dry)
EX-LMO	–5.4 (wet)	+7.3 ± 7.5 (wet)	+10.1 (wet)
	–4.7 (dry)	–5.6 ± 3.6 (dry)	–3.6 (dry)

4 Supplementary Discussion

Selection and length of simulation periods

April 2006 and August 2005 represent typical months of the main wet season (March-May) and the main dry season (June/July-September), respectively, in equatorial East Africa, with regard to a 30-year (1979-2008) climatological period. Details of this selection are in Mölg and Kaser (2011).

It is impossible to quantify the error in results due to the exact choice of the time window, but the two seasonal frequency distributions of the 30 years show a well defined peak region in which the chosen months are located. Thus it is unlikely that they do not represent the most common case of results. Mean monthly precipitation over the larger Kilimanjaro region in April 2006 and August 2005 amounted to 4 and 0.6 mm day^{-1}, respectively, and the 30-year statistics for minimum, percentiles 25 and 75, and maximum are [0.4 2.5 5.7 10.5] for the March-May wet season and [0.1 0.4 0.9 5.7] for the June-September dry season.

A length of one month for the simulations has been used in other atmospheric model studies on LCC for the determination of seasonal sensitivities (Pitman et al., 2004). This allows consideration of feedbacks from variables with a longer memory than the atmosphere. It concerns in particular soil moisture, since the sensitivity of evapotranspiration to soil moisture is an important parameter in the land-atmosphere system. Teuling et al. (2006) showed from measurements that the strongest sensitivities occur in the absence of rainfall and within a time scale of one month. Only weak sensitivities act on time scales longer than one month, but these have a small effect on evapotranspiration (and thus precipitation) in land surface models (e.g., Fig. 3 in Teuling et al., 2006).

Importance of changes in glacier extent for the summit climate change

In experiment EX-REF, we also made one run (for each wet and dry season) where the land cover of 2000 is used together with the glacier extent of 1976 (LC_{2000} but with the six white grid cells in Fig. S1, left). This shows negligibly small changes of atmospheric conditions on the summit compared to LC_{2000} with the recent glacier extent (Fig. S1, right) in both seasons. Small implications are evident for precipitation, where the decrease in glacier extent in the atmospheric model decreases simulated monthly precipitation on the summit by 1.3 mm in the wet season (compared to a 5.7 mm decrease due to the full land cover change, Tab. S4). In the dry season there is no obvious effect.

The potential of local land cover change in forcing summit climate

We conducted one hypothetical model run for the wet season and EX-LMO settings (strongest glacier response case, see Tab. 1 in main text), where all deciduous and evergreen forest is replaced by grassland. This deforestation scenario was defined by Fairman et al. (2011). Results show that precipitation decrease in the "former" forest zone (1750-3750 m) is slightly stronger than due to the observed LCC in Fig. 4 of the paper, by roughly 6 mm $month^{-1}$ on average. In the summit zone (> 5500 m) the complete deforestation effect is reduced: mean precipitation is affected by 2 mm $month^{-1}$, and hardly shows change at the Kersten Glacier location (+1 mm). Thus from a model perspective the large-scale forcing of –31 ± 11 mm $month^{-1}$ (see main text) could never be reached, even if the characteristic LCC on Kilimanjaro (forest loss) would continue to its extreme.

5 Supplementary Notes

This work was funded by the Austrian Science Fund (FWF: P20089-N10, P22106-N21, P22443-N21), the University of Innsbruck's "Nachwuchsförderung", the Tyrolean Science Fund, and the "Deutsche Forschungsgemeinschaft" (A.H.). The supercomputing was supported by the Austrian Ministry of Science BMWF as part of the "UniInfrastrukturprogramm" of the "Forschungsplattform" Scientific Computing at LFU Innsbruck. Local authorities in Tanzania (COSTECH, KINAPA, TANAPA, TAWIRI) granted research permits for our field work. We sincerely thank three anonymous reviewers who provided excellent, constructive comments on the original manuscript.

References in Supplementary Material

Chen F., Dudhia J. (2001): Coupling an advanced land surface-hydrology model with the Penn State-NCAR MM5 modeling system. Part I: Model implementation and sensitivity. *Monthly Weather Review*, **129**: 569-585.

Fairman J.G., Nair U.S., Christopher S.A., Mölg T. (2011): Land use change impacts on regional climate over Kilimanjaro. *Journal of Geophysical Research*, **116**: D03110.

Hemp A. (2005): Climate change driven forest fires marginalize the impact of ice cap wasting on Kilimanjaro. *Global Change Biology*, **11**: 1013-1023.

Hemp A. (2006): Vegetation of Kilimanjaro: hidden endemics and missing bamboo. *African Journal of Ecology*, **44**: 305-328.

Mölg T., Cullen N.J., Hardy D.R., Winkler M., Kaser G. (2009): Quantifying climate change in the tropical mid-troposphere over East Africa from glacier shrinkage on Kilimanjaro. *Journal of Climate*, **22**: 4162-4181.

Mölg T., Kaser G. (2011): A new approach to resolving climate-cryosphere relations: Downscaling climate dynamics to glacier-scale mass and energy balance without statistical scale linking. *Journal of Geophysical Research*, **116**: D16101.

Pitman A.J., Narisma G.T., Pielke Sr. R.A., Holbrook N.J. (2004): Impact of land cover change on the climate of southwest Western Australia. *Journal of Geophysical Research*, **109**: D18109.

Rotach M.W., Zardi D. (2007): On the boundary layer structure over highly complex terrain: Key findings from MAP. *Quarterly Journal of the Royal Meteorological Society*, **133**: 937-948.

Sertel E, Robock A, Ormeci C (2010): Impacts of land cover data quality on regional climate simulations. *International Journal of Climatology*, **30**: 1942-1953.

Skamarock W.C., Klemp J.B., Dudhia J., Gill D.O., Barker D.M., Duda M.G., Huang X.Y., Wang W., Powers J.G. (2008): A description of the Advanced Research WRF Version 3. *NCAR Technical Note*: NCAR/TN-475+STR.

Smirnova T.G., Brown J.M., Benjamin S.G. (1997): Performance of different soil model configurations in simulating ground surface temperature and surface fluxes. *Monthly Weather Review*, **125**: 1870-1884.

Teuling A.J., Seneviratne S.I., Williams C., Troch P.A. (2006): Observed timescales of evapotranspiration response to soil moisture. *Geophysical Research Letters*, **33**: L23403.